



HAL
open science

Lignocellulosic fiber breakage in a molten polymer. Part 3. Modeling of the dimensional change of the fibers during compounding by twin screw extrusion

F. Berzin, J. Beaugrand, S. Dobosz, T. Budtova, Bruno Vergnes

► To cite this version:

F. Berzin, J. Beaugrand, S. Dobosz, T. Budtova, Bruno Vergnes. Lignocellulosic fiber breakage in a molten polymer. Part 3. Modeling of the dimensional change of the fibers during compounding by twin screw extrusion. *Composites Part A: Applied Science and Manufacturing*, 2017, 101, pp.422-431. 10.1016/j.compositesa.2017.07.009 . hal-04057672

HAL Id: hal-04057672

<https://hal.science/hal-04057672>

Submitted on 4 Apr 2023

HAL is a multi-disciplinary open access archive for the deposit and dissemination of scientific research documents, whether they are published or not. The documents may come from teaching and research institutions in France or abroad, or from public or private research centers.

L'archive ouverte pluridisciplinaire **HAL**, est destinée au dépôt et à la diffusion de documents scientifiques de niveau recherche, publiés ou non, émanant des établissements d'enseignement et de recherche français ou étrangers, des laboratoires publics ou privés.

Lignocellulosic fiber breakage in a molten polymer. Part 3. Modeling of the dimensional change of the fibers during compounding by twin screw extrusion

F. Berzin^{a*}, J. Beaugrand^a, S. Dobosz^a, T. Budtova^b, B. Vergnes^b

^aUMR FARE (Fractionnement des AgroRessources et Environnement), Université de Reims
Champagne-Ardenne, INRA, 2 esplanade Roland-Garros, 51686 Reims, France

^bMINES ParisTech, PSL Research University, CEMEF (Centre de Mise en Forme des
Matériaux), UMR CNRS 7635, CS 10207, 06904 Sophia Antipolis Cedex, France

* Corresponding author: F. Berzin

francoise.berzin@univ-reims.fr, Tel.: (33) 3 26 91 84 77

Abstract

In Part 1 and Part 2 of this series, models describing lignocellulose fiber breakage during melt mixing process have been established. In Part 3, these models are applied to predict fiber size when compounding composites in a twin-screw extruder. A comparison with the experimental values of fiber dimensions in composites made under different processing conditions is performed. Various types of fibers (flax, hemp and sisal) with different initial morphologies and sizes were considered in order to show the generality of the approach. First, experimental results, highlighting the main impact of processing parameters on the fiber dimensions, are presented. A particular interest was paid on the change of fiber length, diameter and aspect ratio (length/diameter) all along the screws. Then, it is shown how flow modeling can help to better interpret these results and lead to a predictive approach of fiber breakage during twin-screw extrusion, in order to optimize the compounding process.

Keywords: A. Natural fibers, A. Polymer-matrix composites, C. Process modeling, E. Extrusion

1. Introduction

From an industrial point of view, thermoplastic composites reinforced by short lignocellulosic fibers are primarily prepared by compounding in co-rotating twin-screw extruders, although there are also a few examples using single-screw extruders [1-3], Buss co-kneaders [4], or counter-rotating twin-screw extruders [5]. Co-rotating twin-screw extrusion, because of its flexibility and its great mixing capabilities, is particularly suitable for the manufacturing of this type of composites [6].

The intrinsic properties of lignocellulosic fibers give them interesting reinforcement potential which is necessary to preserve during the preparation of the composite [7]. However, when submitted to the thermomechanical treatment, fibers undergo a decrease in both diameter (separation of bundles into individual fibers) and length (breakage of bundles and single fibers) [8-14]. It is therefore very important to understand how fiber dimensions evolve during the extrusion process and how to optimise the processing conditions (screw profile, screw speed, feed rate, and control barrel temperatures) to promote bundle separation rather than length reduction. This is important for maintaining the highest possible length (L) and aspect ratio (length/diameter, L/D), in order to obtain better mechanical properties.

In Part 1 [15] and Part 2 [16] of this series of papers, we have presented qualitative rheo-optical observations of fiber breakage mechanisms and quantitative laws describing the changes in fiber dimensions during mixing with a polypropylene matrix, respectively. In this Part 3, this knowledge is applied to the understanding of the dimensional changes of various types of fibers during the twin-screw extrusion process.

To limit fiber damage during compounding, a first possibility is to introduce them after the melting of the matrix. Indeed, the melting of the polymer pellets in twin-screw extrusion requires large energy input, leading to high local stresses and strains [17], which is very detrimental to the dimensions of the fibers. This was clearly demonstrated by Berzin et al. [18], Doumbia et al. [4] and Teuber et al. [19]. To avoid this problem, the fibers are usually fed through a secondary feeder located after the melting zone. However, the correct feeding (i.e. accurate and stable in time) of lignocellulosic fiber poses a number of technical problems. Indeed, depending on fiber length and flexibility, they can entangle or wrap around the axes of

the feeder. This induced a number of manufacturers to develop their own feeding systems. However, the incorporation of lignocellulosic fibers into the screw channels remains problematic, especially for small scale extruders and when rather high percent of fiber is used in industrial applications (typically around 30% by weight) [20]. Moreover, the problem is aggravated by the low density of fibers and thus their significant volume. Some authors have proposed fiber pelletizing to increase their bulk-density, but this leads to severe fiber degradation [21]. The processing of long continuous fibers could be an alternative to feeding problems [22, 23], but it is out of the scope of this paper.

Once the fibers are introduced, the challenge is then to disperse them homogeneously in the matrix, while limiting their breakage. As shown in Part 1 [15] and in Part 2 [16], the breakage mechanisms and kinetics depend on the type of fiber (botanical origin, which determines the chemical composition and morphology), its initial dimensions (long fibers break faster) and environment (water content, temperature) [14]. In addition to the aspects related to fiber morphological properties, processing temperatures above fiber decomposition temperature must be avoided. While cellulose degrades around 330-350°C, other components are more temperature sensitive and temperatures above 200°C should be avoided, especially for long residence times [25-28]. Such temperatures are readily reached during an extrusion process, especially for technical polymers. This point is particularly important since, depending on the screw profile, the maximum temperature can be reached not at the extruder end, but somewhere inside the machine (e.g., in kneading discs), and thus can be completely “invisible” to the operator.

The technical review outlined above shows that preparation of composites with lignocellulosic fibers by twin-screw extrusion under conditions that respect their integrity is a real scientific challenge, for which the contribution of modeling can be of great interest. Therefore, in the present paper, we first present experimental observations of the dimensional changes undergone by the fibers along the screw profile under various processing conditions. Then, based on the flow modeling of the extrusion process, we show how the experimental results can be interpreted and, finally, a theoretical prediction of the changes in fiber dimensions (length L , diameter D , aspect ratio L/D) during the compounding process is developed.

2. Materials and methods

2.1 Materials

The matrix used is a high impact polypropylene (PP) for injection molding. It has a melt index of 15 g/10 min (230°C, 2.16 kg). To improve the fiber-matrix interface, maleic anhydride grafted polypropylene (PP-g-MA) is usually employed as compatibiliser [29, 30]. In our experiments, the ratio PP-g-MA/fiber 1/10 in weight was used, as recommended in literature [9, 31, 32].

The fibers were provided by FRD[®] company (Fibres Recherche Developement[®], Troyes, France). Technical flax of two different initial lengths, 4 and 12 mm, sisal of 12 mm and technical retted hemp of 3 mm were used. The initial dimensions of these fibers are shown in Table 1; they were measured as described in Section 2.3. This selection of fibers allows investigation of the effects of the initial length for a given fiber (here, flax) and of the botanical origin for a given initial length (flax and hemp for short fibers, and flax and sisal for long fibers). The composition of the composites remained constant during the study and was fixed as follows (in weight): 78% PP / 2% PP-g-MA / 20% fibers.

2.2 Compounding

The twin-screw extruder used is a co-rotating laboratory-scale machine (Clextral BC21, Firminy, France), with diameter 25 mm and length 900 mm. It includes nine barrel elements (corresponding to nine zones, numbered from 1 to 9, from hopper to screw end, see the profile in Figure 1). In addition to screw conveying elements, it comprises a left-handed element in zone 3 to ensure the melting of the polymer matrix and two mixing blocks in zones 6 and 8, to disperse the fibers. The first one is constituted of five bilobal kneading discs, staggered at 90°. The second one is more restrictive: it also includes five bilobal kneading discs, but staggered at -45°.

The matrix (pre-blend of PP and PP-g-MA pellets) is introduced in zone 1, melted in the left-handed element (zone 3) and the fibers are then added in zone 4. During all experiments, the barrel temperature was kept constant at 180°C (except zone 1 at 80°C and zone 2 at 120°C) and flow rate (2, 4 and 6 kg/h) and screw speed (100 and 200 rpm) were varied. We intentionally limited processing at low speeds to minimize fiber breakage.

To better understand the evolution of fiber breakage along the screws, “dead-stop” experiments were performed: once steady state conditions were reached, the feeding and screw rotation were abruptly stopped, the barrel was cooled down and extracted, and samples were then taken at different locations, indicated by arrows in Figure 1

2.3 Quantification of fiber dimensions

Quantifying the dimensions of lignocellulosic fibers before and after compounding may be performed by different methods, but still remains a delicate task [34]. The results presented here were obtained after dissolving the matrix in Decalin (decahydronaphtalene), acquiring images with a high resolution scanner (Epson Perfection[®] V550) and analysis of these images with ImageJ software. Details on the method can be found elsewhere [34]. Size distributions in length (L), diameter (D) and aspect ratio (L/D) were then obtained. From these distributions, average values can be calculated in different ways. In the following, we will focus on the weight average values (subscript “w”), which give more significance to the high values of the distribution. They are defined by:

$$L_w = \frac{\sum_{i=1}^{N_c} n_i L_i^2}{\sum_{i=1}^{N_c} n_i L_i}, \quad D_w = \frac{\sum_{i=1}^{N_c} n_i D_i^2}{\sum_{i=1}^{N_c} n_i D_i}, \quad (L/D)_w = \frac{\sum_{i=1}^{N_c} n_i (L/D)_i^2}{\sum_{i=1}^{N_c} n_i (L/D)_i} \quad (1)$$

where N_c is the number of classes and n_i the number of fibers of length L_i (or diameter D_i or aspect ratio $(L/D)_i$, respectively).

3. Experimental results: Change of the fiber dimensions along the screws

3.1 General presentation

As mentioned above, samples are collected after stopping the extruder, then cooling and extracting the barrel. An example of results is shown in Figure 2 for the 12 mm flax fibers at 2 kg/h and 100 rpm. The position of the five sampling points is indicated here from the point of introduction of the fibers (zone 4).

A significant reduction (more than a factor 2) of the length and diameter of the fibers is observed as soon as they are introduced and start to be mixed with the molten matrix. This occurs in the screw conveying elements, before the first block of kneading discs. Afterwards, this change is more moderate, but continues until the end of the screws. Although studies of this

type are currently very limited in the literature, similar results were recently reported by Berzin et al. [18], El-Sabbagh et al. [32] and González-Sánchez and González-Quesada [33].

As fiber length and diameter may vary independently, it is not obvious to foresee the change in aspect ratio $(L/D)_w$. Indeed, it can decrease but could also increase if bundles separation is faster than breakage. Figure 3 shows that, despite the very rapid decrease in the diameter observed since the introduction of the fibers of flax 12 mm (Figure 2b), there is a regular decrease of the aspect ratio, indicating that breakage in length remains dominant compared to the bundles separation. All measured parameters (L_w , D_w and $(L/D)_w$) seem to tend towards a limiting value at the end of the extruder, indicating a minimum size below which no decrease is possible under the chosen processing conditions. As it can be seen in Figures S1 to S3 in Supplementary Data, similar results were obtained with the other fibers, with some exceptions that will be commented further.

3.2 Influence of screw speed

The effect of screw speed on changes in length and diameter along the screws for the retted hemp fibers is shown in Figure 4. If an increase in speed leads to lower final values, the change along the screws is not always easy to interpret. Indeed, for the same axial position, the sample may be subjected to higher stresses, but with shorter residence times. The need for a theoretical model to follow the thermomechanical history undergone by the fibers appears thus clearly. Anyway, the effect of screw speed on final length corresponds to the findings in literature, regardless of the nature of the fibers or the mixing process: co-rotating twin-screw extruder [24, 32], counter-rotating twin-screw extruder [35], or internal mixer [19, 36, 37]. Screw speed has a similar influence on the diameter of the bundles (Figure 4b). From the initial 155 μm for the retted hemp, it falls to around 110 and 90 μm for 100 and 200 rpm, respectively. This clearly involves bundles partial separation, but it is still incomplete since the diameter of the individual fiber is not reached (from 10 to 20 μm approximately). This reduction in diameter with the increase in screw speed is also in agreement with the results of the literature [10, 38, 39]. Similar trends were obtained with the other fibers (flax and sisal). Final fiber dimensions are indicated in Table 2 for all processing conditions tested.

3.3 Influence of feed rate

For the same fiber (3 mm retted hemp), the effect of varying feed rate at constant screw speed (200 rpm) is shown in Figure 5. Here also, the change along the screws is complex and it is difficult to understand the role of a particular type of screw element. Depending on its location along the profile and processing conditions, a conveying element may cause more breakage or separation than a mixing element. We can see once again that it is the thermomechanical history undergone by the fiber from its introduction into the extruder that is to follow and assess. Concerning the fiber length, the final value is higher at higher feed rate. This can be explained by a shorter residence time in the mixing zones at a similar stress level and has already been reported in the literature for lignocellulosic fibers [24], but also for glass fibers [40]. The same interpretation applies to changes in length with mixing time in an internal mixer [37, 38].

The variation of diameter is rarely reported in the literature. Figure 5b shows weak influence of feed rate, with large uncertainty in the experimental values due to the difficulty of measuring such parameter [34]. Anyway, the largest final diameter is also obtained for the highest feed rate, i.e. the shortest residence time in the mixing zones.

Similar results were obtained for the other fibers (see Table 2).

All these experimental results show the necessity to better interpret the changes along the screws by estimating the local flow parameters, as temperature, shear rate, shear stress, residence time, strain, etc. For this, the flow modeling appears inevitable.

4. Theoretical approach and modeling

4.1 Flow calculation along the screws

To calculate the flow parameters along the screws, we use the Ludovic[®] software developed about twenty years ago by CEMEF (MINES ParisTech) and INRA [41] and marketed by SCC company (Sciences Computers Consultants, Saint Etienne, France). It is a 1D model based on continuum mechanics, which solves the Stokes equations within the framework of simplified geometry and kinematics, to simulate the whole extrusion process, from the introduction of solid polymer pellets in the hopper to the die exit. This software has been extensively validated by both experimental approaches [42] and comparisons with more

elaborated 3D models [43]. It has already been successfully used to predict the breakage of glass fibers during compounding operations [40, 44, 45] and was also used by Berzin et al. [18] for a first approach of the breakage of lignocellulosic fibers.

Ludovic[®] will be used to estimate the parameters which control the changes of the fiber dimensions. In the literature, cumulative strain and specific mechanical energy (SME) have been proposed to explain the breakage of lignocellulosic fibers [24, 46]. However, it has been shown in Part 2 of this series of publications [16] that the cumulative strain is the adequate parameter to quantify fiber breakage. Therefore, we will focus uniquely on this parameter. Local strain is the product of the local shear rate by the corresponding local residence time. It is then cumulated from the introduction of the fibers to the considered sampling point.

To carry out the simulation, it is necessary to know the rheological behaviors of the matrix and of the composite. Figure 6 shows an example of complex viscosity curves measured for the matrix (PP/PP-g-MA) and for the composite with 12 mm flax fibers. The matrix follows the classical behavior of a thermoplastic polymer, described by a Carreau-Yasuda law, while the composite has a much higher viscosity (a factor ten at low frequency), with a power-law behavior. These results are typical for composites based on lignocellulosic fibers [4, 24, 31, 47, 48]. The viscosity of the composite depends essentially on the fiber content and, at the same fiber content, on the flexibility of the fibers, i.e. their aspect ratio and their elastic modulus. For the fibers tested here, the viscosities of the different composites were very close.

For the simulations with Ludovic[®] software, the viscous behavior of the matrix (Carreau-Yasuda law) is used between the hopper and the point of introduction of the fibers, and that of the composite (power law) further. In order to validate the simulations, the values of final temperature and SME measured on the laboratory extruder (using a thermocouple at the die exit and from the motor torque, respectively) were compared to those calculated by Ludovic[®] software, both for the single matrix and the composite with 3 mm hemp fibers (Figure 7). The agreement is very satisfactory and allows the use of simulation with confidence for the interpretation of the experimental results.

4.2 Change of fibers dimensions along the screws

First, for the case of the 4 mm flax fibers extruded at different feed rates (2, 4 and 6 kg/h) and screw speeds (100 to 200 rpm) is considered. If the values of weight average length measured for the various conditions and the different sampling locations are plotted as a function of the calculated cumulative strain (Figure 8), a master curve is obtained, similar to the case when composites were prepared with the internal mixer [16]. Of course, there is some data dispersion, which is essentially related to the difficulty of accurately measuring the fiber dimensions [34, 49], but this representation confirms that the change in length can be described by an exponential law, as it was originally proposed for glass fibers [40, 50] and later on for lignocellulosic fibers [18, 24]:

$$L_w = L_\infty + (L_0 - L_\infty) \exp(-k_{L_r} \Gamma) \quad (2)$$

where L_0 is the initial fiber length, L_∞ is its ultimate length, Γ is the cumulative strain and k_{L_r} is a constant, quantifying breakage kinetics. In the case of 4 mm flax fibers, we got a good fit of the experimental data with: $L_0 = 4$ mm, $L_\infty = 1.2$ mm and $k_{L_r} = 1.1 \times 10^{-3}$.

This approach can be applied in the same way to the changes in weight average diameter. Figure 9 shows that here also the experimental data fall on a single curve, described by the same type of law:

$$D_w = D_\infty + (D_0 - D_\infty) \exp(-k_{D_r} \Gamma) \quad (3)$$

where D_0 is the initial fiber diameter, D_∞ is its ultimate diameter, and k_{D_r} is a constant quantifying breakage kinetics. We obtained here $D_0 = 242$ μm , $D_\infty = 100$ μm , $k_{D_r} = 2.8 \times 10^{-3}$. These results show that the separation of the bundles is faster than fiber breakage in length (higher value of the kinetic constant), but it does not lead to a full separation into the elementary fibers as the final diameter is about 100 μm .

If we now consider the aspect ratio $(L/D)_w$, we see in Figure 10 that its dependence on cumulative strain is non-monotonous and thus cannot be described by a single exponential law. This non-monotonous evolution was globally observed for the various fibers we tested (see

Figure S4 in Supplementary Data). This is due to the fact that the kinetics of fiber length and diameter changes are not the same.

Moreover, each bundle can break and/or split differently at the same location along the extruder, according to its own dimensions. It is therefore the overall size distributions (both in length and in diameter), and not only average values, that should be followed at any moment during the process. It was done in the case of glass fibers [44], but this case is much simpler because only the length varies and breakage mechanisms are well established. For lignocellulosic fibers of various origins, it was shown using rheo-optics that they break according to different mechanisms [15]. In addition, the kinetics of fiber breakage depends on fiber initial dimensions and “pre-treatment”: for example, bundles of retted fibers were separated faster than non-retted ones [16]. Today, in absence of an accurate mechanistic model of lignocellulosic fibers breakage, we remain limited to the prediction of average values of lengths and diameters.

4.3 Influence of initial fiber morphology and botanical origin

The approach described above can be applied to define the influence of the initial length of the fibers and of their botanical origin. Figure 11 shows the change of length of flax fibers with initial length of 4 and 12 mm. It appears that the long fibers break and separate faster, but they globally result in higher lengths and smaller diameters, i.e. higher aspect ratios. At high strain (above 2000), a large uncertainty is observed for the long fibers. However, it is clear that, at a fixed strain, flax 12 mm is always longer than flax 3 mm. Similar results were also reported by Quinjano-Solis et al. [25], Ausias et al. [1] and Muthuraj et al. [51]. It confirms the interest to use preferentially longer fibers, although their dimensions are greatly reduced during the process.

If now fibers with similar initial length (3.3 and 4 mm) but of different origin (retted hemp and flax) are compared, we see in Figure 12 that the mechanisms of separation and breakage are very different. Hemp breaks much more rapidly than flax, but both reach the same final length values, around 1.2 mm, after a strain of 3000. In contrast, flax fibers separate quickly, starting with higher initial diameter values (242 μm and 155 μm for flax and hemp, respectively), but the two fibers again reach similar diameter values (100-110 μm) at large strain.

Let us now consider flax and sisal fibers with the initial length of 12 mm (Figure 13). It is found that the behaviors are also very different: while flax breaks and separates into thinner bundles rapidly, sisal breaks less and practically does not separate, even at very high strain. This explains why the change of aspect ratio $(L/D)_w$ with cumulative strain is more regular with sisal (see Figure S4c in Supplementary Data). This impact of the botanical origin is essentially due to differences in composition (cellulose, lignin, etc.) and fiber morphology, involving different flexibilities and breakage mechanisms, as explained in Part 1 of this series [15].

If, as mentioned above, the cumulative strain does not allow to always correctly interpret the evolution of the aspect ratio $(L/D)_w$, it permits, however, an overall comparison between fibers for different processing conditions (see Figure S4 in Supplementary Data). For example, whatever the processing conditions, even for large strain, the 4 mm flax fibers have always a greater aspect ratio than the 3 mm hemp ones. Similarly, 12 mm flax fibers have globally better aspect ratios than 12 mm sisal fibers. Finally, 12 mm flax fibers are often better than those of 4 mm flax. If looking for fiber high aspect ratios in composites, it will thus be advantageous to choose i) flax fibers over another type, ii) to prefer initially long fibers and iii) to remain in low strain conditions during the process (ideally, less than 1000).

4.4 Computation of fiber dimensions changes along the screws

We will now show how the previous results can be used to define a semi-predictive model of the change of the dimensions of lignocellulosic fibers during compounding, which can then be used for optimization or scale-up (extrapolation from a laboratory scale to an industrial one).

To develop such a model, it is necessary to couple a twin-screw flow modeling software (here, Ludovic[®] software) with the evolution laws for lengths and diameters. Eqs. (2) and (3), which reflect these changes as a function of cumulative strain, will be used. Of course, any other type of law could be used, provided it defines trends based on a process parameter which can be calculated by Ludovic[®] software (SME, for example).

First, the variation of thermomechanical parameters along the screws is calculated. For example, Figure 14a shows the variation of the cumulative strain along the screw profile. Strain significantly increases in the melting zone and, after the introduction of the fibers, in the two mixing zones. Then, from these data, the evolution of the selected parameter can be calculated

(for example, the weight average length L_w for 4 mm flax), using the corresponding equation (here, Eq. (2)). The result is shown in Figure 14b. We observe a rapid decrease of fiber length along the conveying zones from the introduction of the fibers, with pronounced “jumps” during the flow in each mixing zone.

Figure 15 compares, for the 4 mm flax fibers, size changes calculated by the model with the experimental points, for both weight average lengths and diameters. We observe that, despite some inevitable differences, the model correctly reflects the experimental size changes. This satisfactory agreement between the model and experiment is also observed for the other fibers and the other processing conditions. Some examples are shown in Figures S5 to S8 in Supplementary Data. This approach can thus be used in a predictive manner to optimize screw profile and processing conditions, and to solve the difficult problems of scale-up.

5. Conclusions

When submitted to a thermomechanical treatment, lignocellulosic fibers are subjected to both a reduction of their diameter by separation of the bundles and a reduction in their length by breakage. These changes are closely related to processing conditions: screw profile, barrel temperature, screw speed, feed rate. They also differ depending on the botanical origin of the fiber and on its initial dimensions. However, size changes can be generally described by exponential laws, which are based on the cumulative strain undergone by the fiber. Using thermomechanical modeling of the twin-screw extrusion process, it is then possible to calculate the variations of length and diameter during the compounding process. This model, once validated, may lead to an understanding of what happens during compounding, to an optimization of the processing conditions and possibly the screw profile for a given fiber size, and also to a solution of the problems of scale-up, i.e. the extrapolation of the processing conditions of an industrial machine from those of a laboratory extruder.

Acknowledgements

This work has been carried out during the DEFIBREX project, funded by the French National Research Agency (ANR-12-RMNP-004), and, for FARE, by the Competitiveness Cluster Industries & Agro-Resources (IAR). We thank the company FRD[®] (Fibres Recherche

Development[®], Troyes, France) for providing the fibers, and all the partners of the DEFIBREX project (Faurecia, KTron, I2M, SCC).

References

- [1] Ausias G, Bourmaud A, Coroller G, Baley C. Study of the fibre morphology stability in polypropylene-flax composites. *Polym Deg Stab* 2013;98:1216-1224.
- [2] Soleimani M, Tabil L, Panigrahi S, Opoku A. The effect of fiber pretreatment and compatibilizer on mechanical and physical properties of flax fiber-polypropylene composites. *J Polym Environ* 2008;16:74-82.
- [3] Silva Spinacé MA, Feroseli KKG, De Paoli MA. Recycled polypropylene reinforced with curaua fibers by extrusion. *J Appl Polym Sci* 2009;112:3686-3694.
- [4] Doumbia AS, Castro M, Jouannet D, Kervoëlen A, Falher T, Cauret L, Bourmaud A. Flax/polypropylene composites for lightened structures: Multiscale analysis of process and fibre parameters. *Mat Design* 2015;87:331-341.
- [5] Bledzki AK, Franciszczak P, Meljon A. high performance hybrid PP and PLA bio-composites reinforced with short man-made cellulose fibres and softwood flour. *Comp Part A* 2015;74:132-139.
- [6] Lafleur PG, Vergnes B. *Polymer Extrusion*, London: ISTE-Wiley, 2014.
- [7] Müssig J. *Industrial Applications of Natural Fibres*. Chichester: John Wiley, 2010.
- [8] Hornsby PR, Hinrichsen E, Tarverdi K. Preparation and properties of polypropylene composites reinforced with wheat and flax straw fibres. Part II Analysis of composite microstructure and mechanical properties. *J Mat Sci* 1997;32:1009-1015.
- [9] Bos HL, Müssig J, van den Oever MJA. Mechanical properties of short-flax-fibre reinforced compounds. *Comp Part A* 2006;37:1591-1604.
- [10] Barkoula NM, Garkhail SK, Peijs T. Effect of compounding and injection molding on the mechanical properties of flax fiber polypropylene composites. *J Reinf Plast Comp* 2010;29:1366-1385.

- [11] Feng Y, Hu Y, Zhao G, Yin J, Jiang W. Preparation and mechanical properties of high-performance short ramie fiber-reinforced polypropylene composites. *J Appl Polym Sci* 2011;122:1564-1571.
- [12] Peltola H, Pääkkönen E, Jetsu P, Heinemann S. Wood based PLA and PP composites: Effect of fibre type and matrix polymer on fibre morphology, dispersion and composite properties. *Comp Part A* 2014;61:13-22.
- [13] Dickson AR, Even D, Warnes JM, Fernyhough A. The effect of reprocessing on the mechanical properties of polypropylene reinforced with wood pulp, flax or glass fibre. *Comp Part A* 2014;61:258-267.
- [14] Feldmann M, Heim HP, Zarges JC. Influence of the process parameters on the mechanical properties of engineering biocomposites using a twin-screw extruder. *Comp Part A* 2016;83:113-119.
- [15] Castellani R, Di Giuseppe E, Dobosz S, Beaugrand J, Berzin F, Vergnes B, Budtova T. Lignocellulosic fiber breakage in a molten polymer. Part 1. Qualitative analysis using rheo-optical observations. *Comp Part A* 2016;91:229-237.
- [16] Di Giuseppe E, Castellani R, Budtova T, Vergnes B. Lignocellulosic fiber breakage in a molten polymer. Part 2: Quantitative analysis of the breakage mechanisms during compounding. *Comp Part A* 2017;95:31-39.
- [17] Vergnes B, Souveton G, Delacour ML, Ainsler A. Experimental and theoretical study of polymer melting in a co-rotating twin screw extruder. *Intern Polym Proc* 2001;16:351-362.
- [18] Berzin F, Vergnes B, Beaugrand J. Evolution of lignocellulosic fibre lengths along the screw profile during twin screw compounding with polycaprolactone. *Comp Part A* 2014;59:30-36.
- [19] Teuber L, Militz H, Krause A. Processing of wood plastic composites: The influence of feeding method and polymer melt flow rate on particle degradation. *J Appl Polym Sci* 2015;43231:1-9.
- [20] Keller A. Compounding and mechanical properties of biodegradable hemp fibre composites. *Comp Sci Tech* 2003;63:1307-1316.

- [21] Bengtsson M, Le Baillif M, Oksman K. Extrusion and mechanical properties of highly filled cellulose fibre-polypropylene composites. *Comp Part A* 2007;38:1922-1931.
- [22] Van den Oever MJA, Snijder MHB. Jute fiber reinforced polypropylene produced by continuous extrusion compounding, Part 1: Processing and ageing properties. *J Appl Polym Sci* 2008;110:1009-1018.
- [23] Oksman K, Skrifvars M, Selin JF. Natural fibres as reinforcement in polylactid acid (PLA) composites. *Comp Sci Tech* 2003;63:1317-1324.
- [24] Beaugrand J, Berzin F. Lignocellulosic fiber reinforced composites: influence of compounding conditions on defibrization and mechanical properties. *J Appl Polym Sci* 2013;128:1227-1238.
- [25] Quijano-Solis C, Yan N, Zhang SY. Effect of mixing conditions and initial fiber morphology on fiber dimensions after processing. *Comp Part A* 2009;40:351-358.
- [26] Summerscales J, Dissanayake NPJ, Virk AS, Hall W. A review of bast fibres and their composites. Part 1 - Fibres as reinforcements. *Comp Part A* 2010; 41:1329-1335.
- [27] Gassan J, Bledzky AK. Thermal degradation of flax and jute fibers, *J Appl Polym Sci* 2001;82:1417-1422.
- [28] Oza S, Ning H, Ferguson I, Lu N. Effect of surface treatment on thermal stability of the hemp-PLA composites: Correlation of activation energy with thermal degradation. *Comp Part B* 2014;67:227-232.
- [29] Gassan J, Bledski AK. The influence of fiber-surface treatment on the mechanical properties of jute-polypropylene composites. *Comp Part A* 1997;28:1001-1005.
- [30] Sun ZY, Han HS, Dai GC. Mechanical properties of injection-molded natural fiber-reinforced polypropylene composites: formulation and compounding processes. *J Reinf Plast Comp* 2010;29:637-650.
- [31] Le Moigne N, van den Oever M, Budtova T. A statistical analysis of fibre size and shape distribution after compounding in composites reinforced by natural fibres. *Comp Part A* 2011;42:1542-1550.

- [32] El-Sabbagh AMM, Steuernagel L, Meiners D, Ziegmann G. Effect of extruder elements on fiber dimensions and mechanical properties of bast natural fiber polypropylene composites. *J Appl Polym Sci* 2014;40435.
- [33] González-Sánchez C, González-Quesada M. Novel automated method for evaluating the morphological changes of cellulose fibres during extrusion-compounding of plastic–matrix composites. *Comp Part A* 2015;69:1-9.
- [34] Di Giuseppe E, Castellani R, Dobosz S, Malvestio J, Berzin F, Beaugrand J, Delisée C, Vergnes B, Budtova T. Reliability evaluation of automated analysis, 2D scanner, and microtomography methods for measuring fiber dimensions in polymer-lignocellulosic fiber composites. *Comp Part A* 2016;90:320-329.
- [35] Alvarez V, Iannoni A, Kenny JM, Vázquez A. Influence of twin-screw processing conditions on the mechanical properties of biocomposites. *Comp Mat* 2005;39:2023-2038.
- [36] Joseph PV, Joseph K, Thomas S. Effect of processing variables on the mechanical properties of sisal-fiber-reinforced polypropylene composites. *Comp Sci Tech* 1999;59:1625-1640.
- [37] Baiardo M, Zini E, Scandola M. Flax fibre-polyester composites. *Comp Part A* 2004;35:703-710.
- [38] Iannace S, Ali R, Nicolai L. Effect of processing conditions on dimensions of sisal fibers in thermoplastic biodegradable composites. *J Appl Polym Sci* 2001;79:1084-1091.
- [39] Mano B, Araújo JR, Spinacé MAS, De Paoli MA. Polyolefin composites with curaua fibres: Effect of the processing conditions on mechanical properties, morphology and fibres dimensions. *Comp Sci Tech* 2010;70:29-35.
- [40] Inceoglu F, Ville J, Ghamri N, Durin A, Valette R, Vergnes B. Correlation between processing conditions and fiber breakage during compounding of glass fiber-reinforced polyamide, *Polym Comp* 2011;32:1842-1850.
- [41] Vergnes B, Della Valle G, Delamare L. A global computer software for polymer flows in corotating twin screw extruders, *Polym Eng Sci* 1998;38:1781- 1792.
- [42] Carneiro OS, Covas JA, Vergnes B. Experimental and theoretical study of the twin screw extrusion of polypropylene. *J Appl Polym Sci* 2000;78:1419-1430.

- [43] Durin A, De Micheli P, Nguyen HC, David C, Valette R, Vergnes B. Comparison between 1D and 3D approaches for twin-screw extrusion simulation, *Intern Polym Proc* 2014;29:641-648.
- [44] Durin A, De Micheli P, Ville J, Inceoglu F, Valette R, Vergnes B. A matricial approach of fibre breakage in twin-screw extrusion of glass fibres reinforced thermoplastics. *Compos Part A* 2013;48:47–56.
- [45] Ville J, Inceoglu F, Ghamri N, Pradel JL, Durin A, Valette R, Vergnes B. Influence of extrusion conditions on fiber breakage along the screw profile during twin screw compounding of glass fiber-reinforced PA, *Intern Polym Proc* 2013;28:49-57.
- [46] Le Duc A, Vergnes B, Budtova T. Polypropylene/natural fibres composites: analysis of fibre dimensions after compounding and observations of fibre rupture by rheo-optics. *Comp Part A* 2011;42:1727-17370.
- [47] Abdennadher A, Vincent M, Budtova T. Rheological properties of molten flax- and Tencel[®]-polypropylene composites: Influence of fiber morphology and concentration. *J Rheol* 2016;60:191-201.
- [48] Mihai M, Chapleau N, Denault J. Processing-formulation-performance relationships of polypropylene/short flax fiber composites. *J Appl Polym Sci* 2015;41528
- [49] Legland D, Beaugrand J. Automated clustering of lignocellulosic fibres based on morphometric features and using clustering of variables. *Ind Crops Prod* 2013;45:253– 261.
- [50] Shon K, Liu D, White JL. Experimental studies and modeling of development of dispersion and fiber damage in continuous compounding. *Intern Polym Proc* 2005;20:322–331.
- [51] Muthuraj R, Misra M, Defersha F, Mohanty AK. Influence of processing parameters on the impact strength of biocomposites: A statistical approach. *Comp Part A* 2016;83:120-129.

Figure captions

Figure 1. Scheme of the laboratory scale twin-screw extruder (Clextral BC21). Restrictive zones are in grey. Arrows indicate sampling locations.

Figure 2. Changes in length (a) and diameter (b) of 12 mm flax fibers along the screws (2 kg/h, 100 rpm). Lines are just to guide the eyes.

Figure 3. Changes in aspect ratio of 12 mm flax fibers along the screws (2 kg/h, 100 rpm). Lines are just to guide the eyes.

Figure 4. Changes in length (a) and diameter (b) of 3 mm retted hemp fibers along the screws for two screw speeds (filled circles: 100 rpm, open circles: 200 rpm, 6 kg/h). Lines are just to guide the eyes.

Figure 5. Changes in length (a) and diameter (b) of 3 mm retted hemp fibers along the screws for three feed rates (filled circles: 2 kg/h, open circles: 4 kg/h, filled squares: 6 kg/h, 200 rpm). Lines are just to guide the eyes.

Figure 6. Complex viscosity curves for the matrix and the composite with 12 mm flax fibers (200 °C).

Figure 7. Comparison between experimental and calculated values for (a) final temperature and (b) specific mechanical energy (SME) (filled circles: matrix, open circles: composite with 3 mm hemp fibers).

Figure 8. Changes in length of 4 mm flax fibers as function of cumulative strain. Symbols are experimental points, the full line is a fit using Eq. (2).

Figure 9. Changes in diameter of 4 mm flax fibers as function of cumulative strain. Symbols are experimental points, the full line is a fit using Eq. (3).

Figure 10. Changes in aspect ratio of 4 mm flax fibers as function of cumulative strain.

Figure 11. Changes in (a) length and (b) diameter of flax fibers of initial length 4 mm (open circles) and 12 mm (filled circles) as function of cumulative strain. Symbols are experimental points, the full lines are fits using Eqs. (2) and (3).

Figure 12. Changes in (a) length and (b) diameter of flax (open circles) and hemp (filled circles) fibers of initial length close to 4 mm as function of cumulative strain. Symbols are experimental points, the full lines are fits using Eqs. (2) and (3).

Figure 13. Changes in (a) length and (b) diameter of flax (open circles) and sisal (filled circles) fibers of initial length close to 12 mm as function of cumulative strain. Symbols are experimental points, the full lines are fits using Eqs. (2) and (3).

Figure 14. Evolutions of calculated (a) cumulative strain and (b) average diameter of 4 mm flax fibers along the screws (6 kg/h, 200 tr/min).

Figure 15. Changes in (a) length and (b) diameter of 4 mm flax fibers along the screws (6 kg/h, 200 rpm). Comparison between theoretical model (lines) and experiments (symbols).

Table 1. Weight average values of length, diameter and aspect ratio of the initial fibers.

	Average length L_w (mm)	Average diameter D_w (μm)	Average aspect ratio $(L/D)_w$ (-)
Hemp 3 mm	3.3	155	20.2
Flax 4 mm	4.0	242	18.8
Flax 12 mm	12.0	248	41.9
Sisal 12 mm	12.3	280	40.1

Table 2. Weight average values of length, diameter and aspect ratio of the fibers in the composites after compounding.

Fiber type	Screw speed (rpm)	Feed rate (kg/h)	Average length L_w (mm)	Average diameter D_w (μm)	Average aspect ratio $(L/D)_w$ (-)
Hemp 3 mm	100	2	1.13	94	9.2
	100	4	1.32	76	11.3
	100	6	1.66	112	10.9
	200	6	1.39	89	11.7
Flax 4 mm	100	2	1.29	95	13.3
	100	4	1.54	100	17.8
	100	6	2.32	114	20.5
Flax 12 mm	100	2	1.67	67	15.7
	100	4	4.22	76	44.2
	100	6	4.81	86	31.1
	200	6	4.29	84	29.1
Sisal 12 mm	100	2	4.91	269	14.3
	200	2	3.70	225	13.8
	100	4	3.20	218	10.3
	200	4	4.10	246	13.9

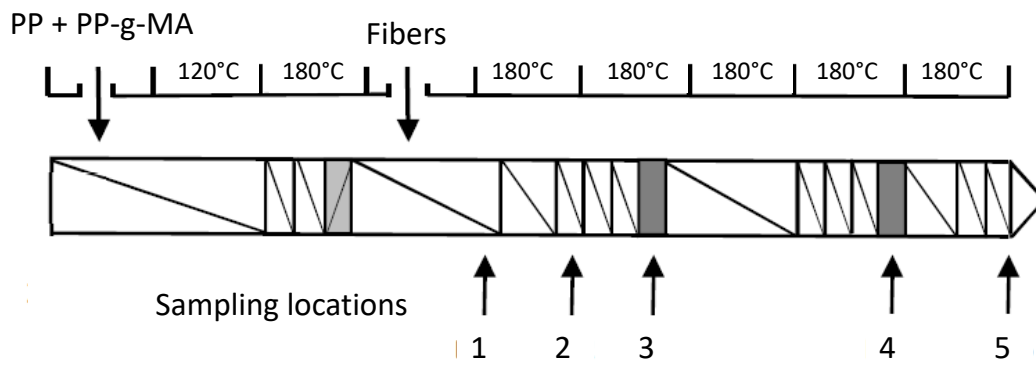


Figure 1. Scheme of the laboratory scale twin-screw extruder (Clextral BC21). Restrictive zones are in grey. Arrows indicate sampling locations.

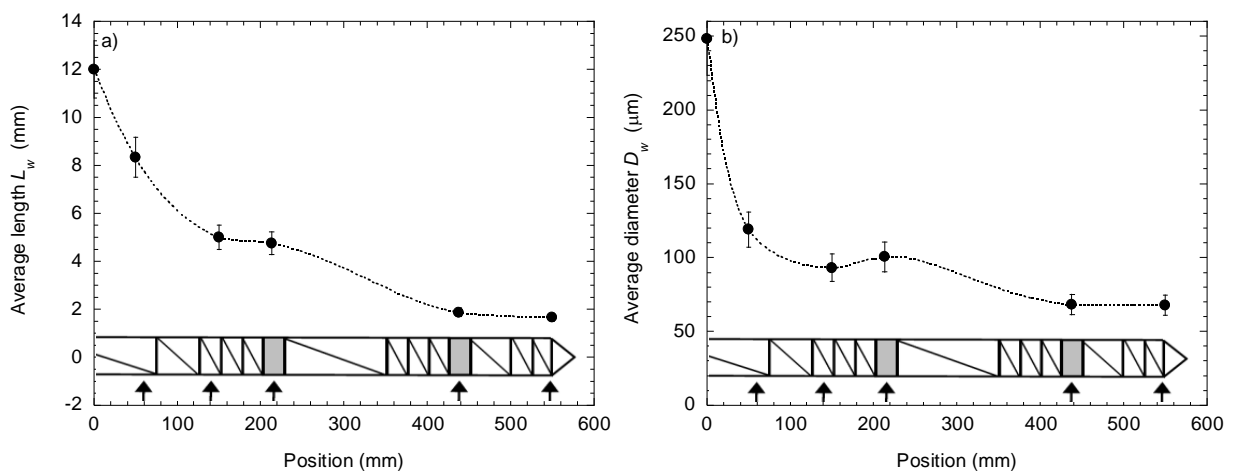


Figure 2. Changes in length (a) and diameter (b) of 12 mm flax fibers along the screws (2 kg/h, 100 rpm). Lines are just to guide the eyes.

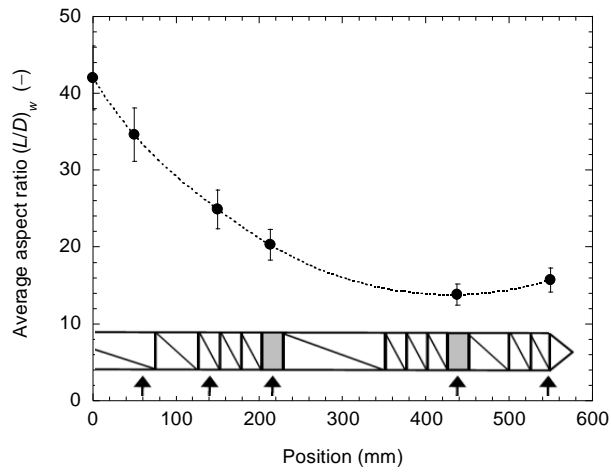


Figure 3. Changes in aspect ratio of 12 mm flax fibers along the screws (2 kg/h, 100 rpm). Lines are just to guide the eyes.

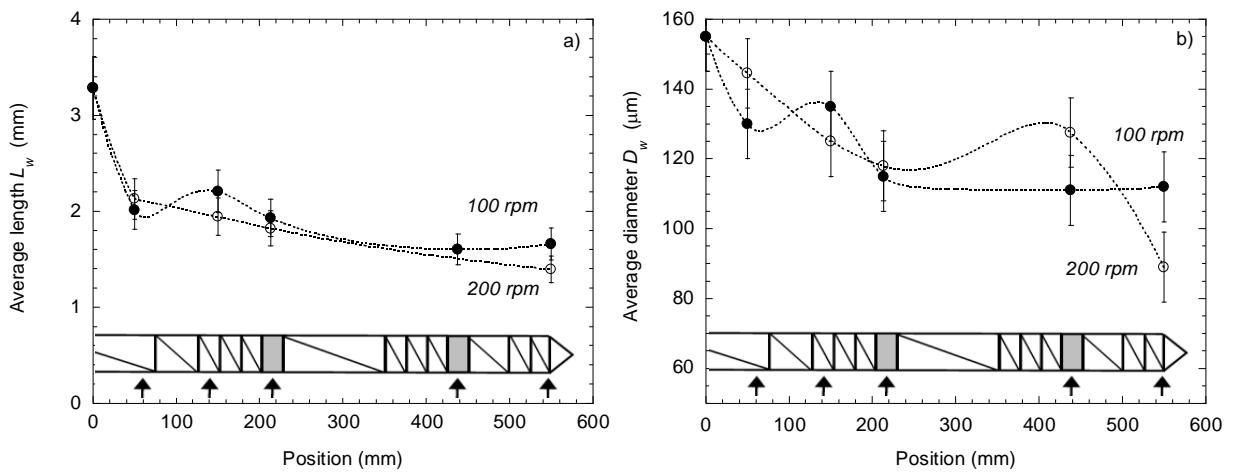


Figure 4. Changes in length (a) and diameter (b) of 3 mm retted hemp fibers along the screws for two screw speeds (filled circles: 100 rpm, open circles: 200 rpm) at 6 kg/h.

Lines are just to guide the eyes.

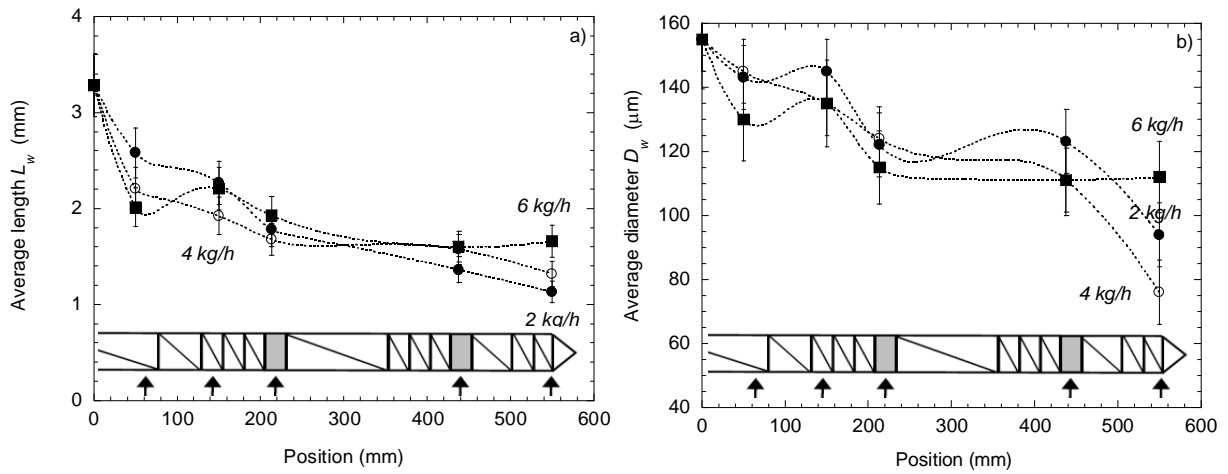


Figure 5. Changes in length (a) and diameter (b) of 3 mm retted hemp fibers along the screws for three feed rates (filled circles: 2 kg/h, open circles: 4 kg/h, filled squares: 6 kg/h) at 200 rpm. Lines are just to guide the eyes.

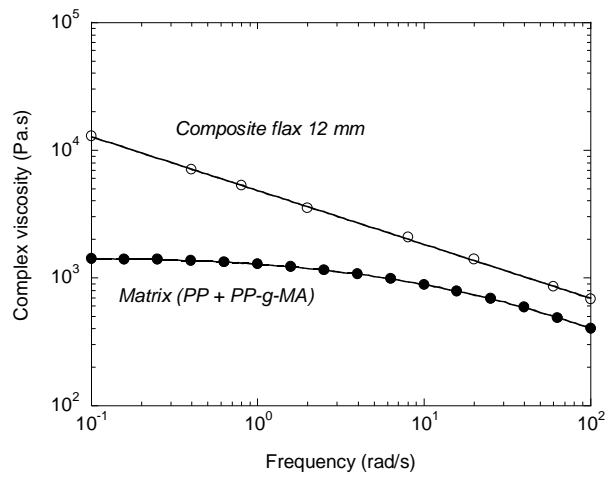


Figure 6. Complex viscosity curves for the matrix and the composite with 12 mm flax fibers (200°C).

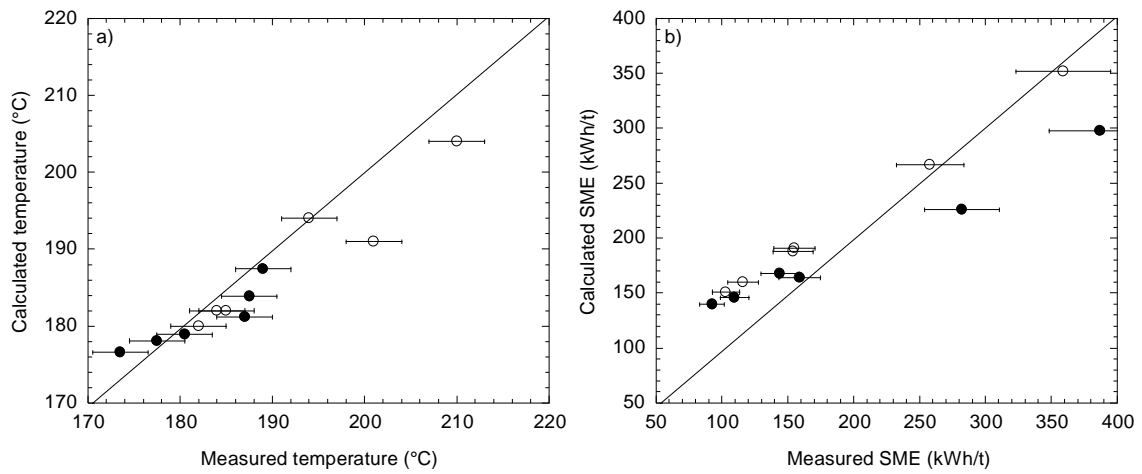


Figure 7. Comparison between experimental and calculated values for (a) final temperature and (b) specific mechanical energy (SME) (filled circles: matrix, open circles: composite with 3 mm hemp fibers).

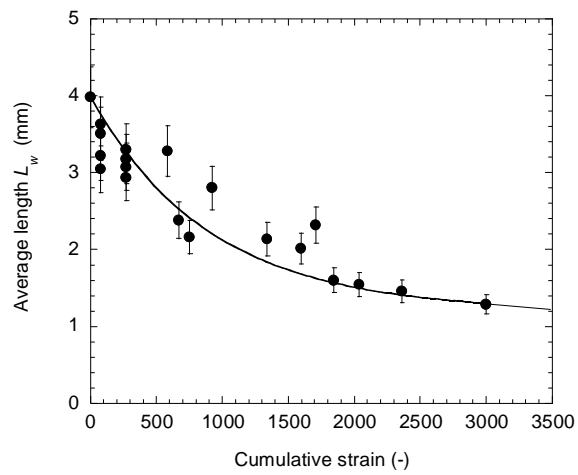


Figure 8. Changes in length of 4 mm flax fibers as a function of cumulative strain.

Symbols are experimental points, the line is a fit using Eq. (2).

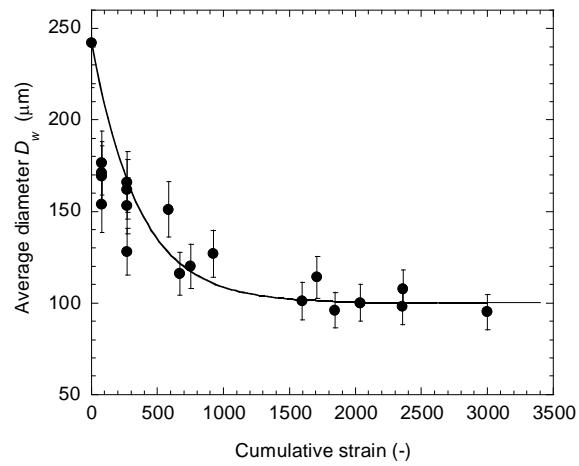


Figure 9. Changes in diameter of 4 mm flax fibers as function of cumulative strain.

Symbols are experimental points, the line is a fit using Eq. (3).

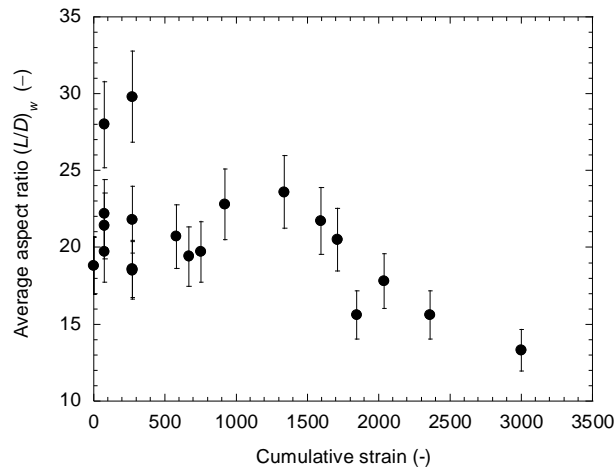


Figure 10. Changes in aspect ratio of 4 mm flax fibers as function of cumulative strain.

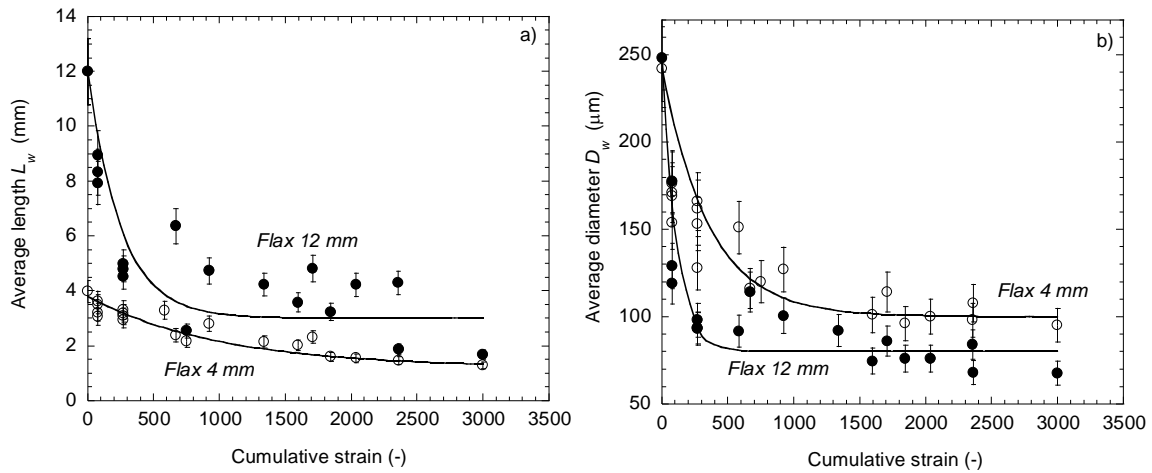


Figure 11. Changes in (a) length and (b) diameter of flax fibers of initial length 4 mm (open circles) and 12 mm (filled circles) as function of cumulative strain. Symbols are experimental points, the lines are fits using Eqs. (2) and (3).

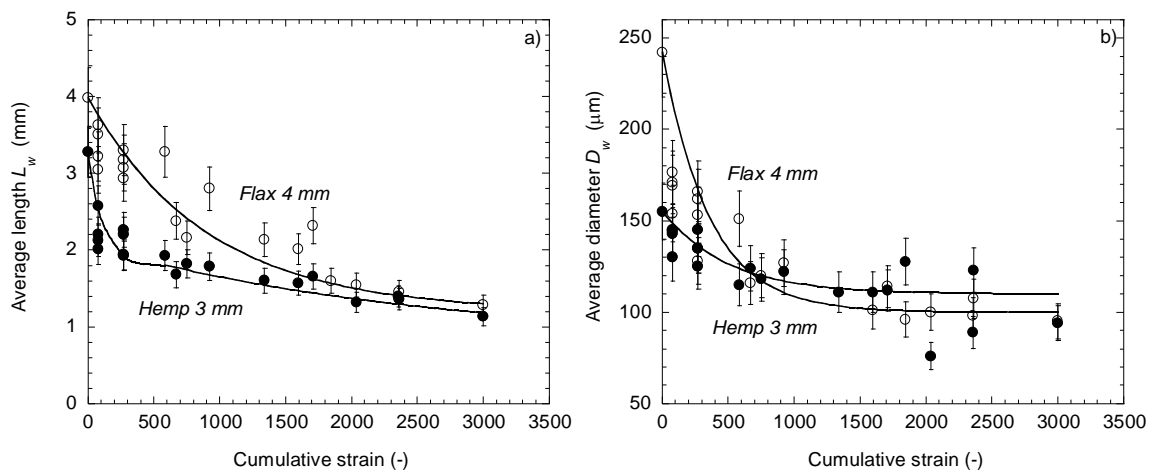


Figure 12. Changes in (a) length and (b) diameter of flax (open circles) and hemp (filled circles) fibers of initial length 4 and 3.3 mm, respectively, as a function of cumulative strain. Symbols are experimental points, the lines are fits using Eqs. (2) and (3).

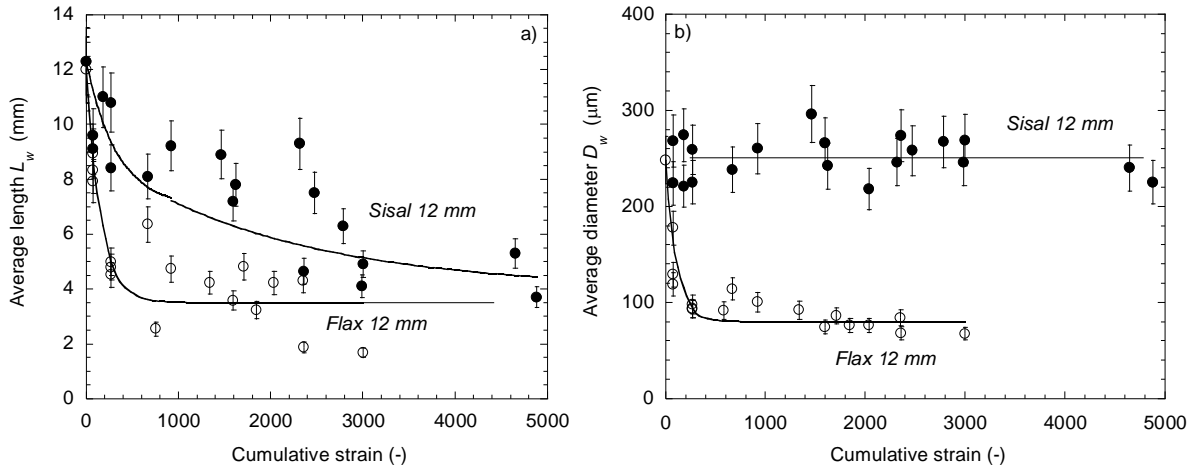


Figure 13. Changes in (a) length and (b) diameter of flax (open circles) and sisal (filled circles) fibers of initial length close to 12 mm as a function of cumulative strain.

Symbols are experimental points, the lines are fits using Eqs. (2) and (3).

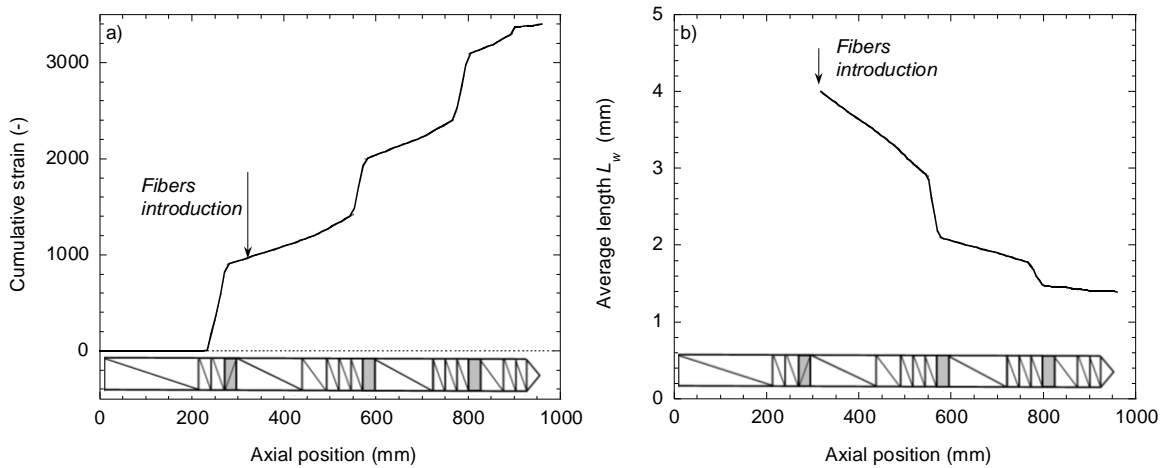


Figure 14. Evolutions of calculated (a) cumulative strain and (b) average length of 4 mm flax fibers along the screws (6 kg/h, 200 rpm)

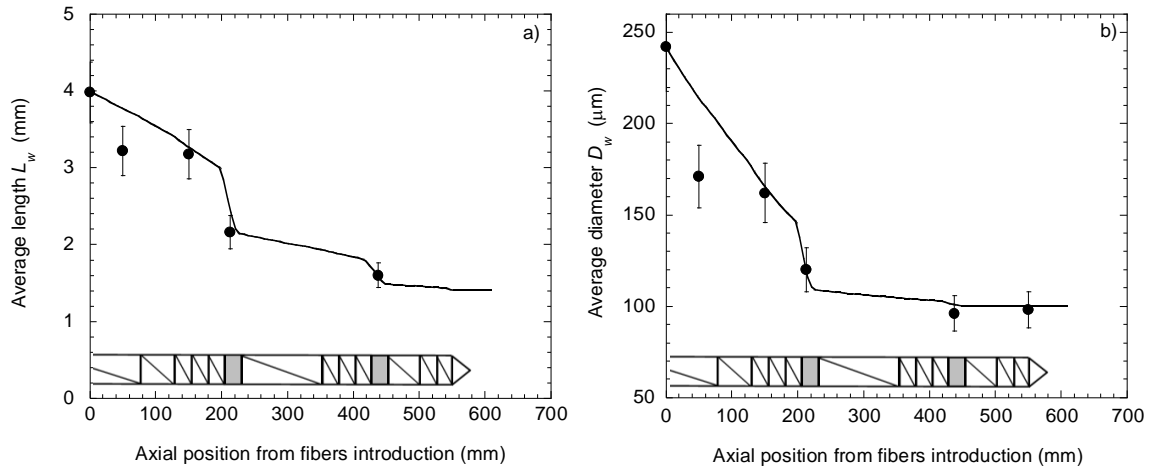


Figure 15. Changes in (a) length and (b) diameter of 4 mm flax fibers along the screws (6 kg/h, 200 rpm). Comparison between theoretical model (lines) and experiments (symbols).